COMPTES RENDUS

PHYSIQUE

Slow-light: Fascinating physics or potential applications?

Artificial dispersion of active optical coupled resonator systems

Stéphane Trebaol [a], Thị Kim Ngân Nguyên [b], Hervé Tavernier [b], Laura Ghişa [a],
Yannick Dumeige [a,*], Patrice Féron [a]

[a] *ENSSAT-FOTON (CNRS-UMR 6082) – Université de Rennes 1, 6, rue de Kerampont, boîte postale 80518, 22300 Lannion, France*
[b] *FEMTO-ST (CNRS-UMR 6174) – Université de Franche-Comté, 16, route de Gray, 25030 Besançon, France*

Abstract

We study both theoretically and experimentally the dispersive properties of single or coupled active resonators. In the case of single resonator systems, we present a simple experimental protocol which allows us to obtain in detail its coupling regime and thus their dispersive properties. We show that the active coupled systems offer some degrees of freedom to tailor the high dispersion orders. All the propositions are experimentally tested using a model system made of Er^{3+} doped fiber ring resonators. These artificial media could be used as tunable or amplifying compact optical delay lines. We also show that the proposed experimental protocol can be applied to passive whispering gallery mode resonators. ***To cite this article: S. Trebaol et al., C. R. Physique 10 (2009).***
© 2009 Académie des sciences. Published by Elsevier Masson SAS. All rights reserved.

Résumé

Dispersion artificielle de systèmes à résonateurs optiques actifs couplés. Nous étudions d'un point de vue théorique et expérimental les propriétés dispersives de systèmes de résonateurs actifs couplés ou non. Dans le cas d'un unique résonateur, nous présentons un protocole expérimental simple qui nous permet de connaître en détail le régime de couplage du résonateur et par conséquent ses propriétés dispersives. Nous montrons que les systèmes de résonateurs actifs couplés offrent suffisament de degrés de liberté pour façonner les différents ordres de dispersion. Toutes les propositions sont testées expérimentalement en utilisant un système modèle fait de résonateurs à fibres dopées Er^{3+}. Ces milieux artificiels pourraient être utilisés comme lignes à retard optiques variables ou amplificatrices. Nous montrons également que le protocole expérimental proposé dans cet article peut aussi être appliqué à des résonateurs à modes de galerie passifs. ***Pour citer cet article : S. Trebaol et al., C. R. Physique 10 (2009).***
© 2009 Académie des sciences. Published by Elsevier Masson SAS. All rights reserved.

Keywords: Coupled resonators; Whispering gallery mode resonators; Selective amplification; Optical delay lines

Mots-clés : Résonateurs couplés ; Résonateurs à modes de galerie ; Amplification sélective ; Lignes à retard optiques

1. Introduction

Most slow-light systems basically rely on the resonant interaction of light and a sharp material resonance. To avoid the absorption associated with strong material dispersion, it has been proposed to use quantum coherence effects such
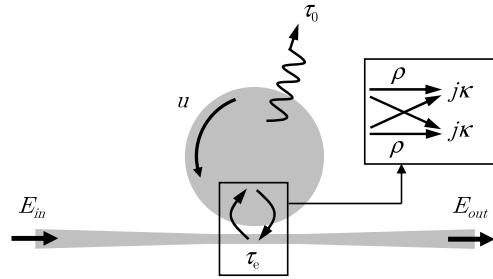
Fig. 1. Optical resonator coupled to a single access line. The input and output fields are E_{in} and E_{out}. u is the mode amplitude, τ_0 is the intrinsic photon lifetime and τ_e is the coupling photon lifetime. The inset represents the amplitude coupling coefficient κ.

as electromagnetically induced transparency [1,2] or coherent population oscillations [3]. The dissipation issue can also be circumvented by using resonant gain. This last effect can be implemented in optical fiber, for example using Brillouin coherent scattering [4]. It has also been proposed to use photonic structures with artificial resonances to reduce the group velocity [5]. A lot of experimental evidences of slowing of light in photonic crystals [6] or coupled resonators systems [7] have been already reported. Indeed, an optical resonator (e.g. Fabry–Perot interferometer, ring resonator, …) can be seen as an optical filter whose phase shift rapidly changes across its resonance introducing a group delay [5]. In this article, we would like to present the dispersive properties of resonators made of active materials. These systems should combine a strong dispersion, low optical losses and even optical gain. We first review the dispersive properties of a single two port optical resonator. We also present a very convenient experimental method allowing all the linear characteristics of passive and active resonators to be simply obtained. In the second part of the article, we experimentally show that the coupling of active resonators offer supplementary degrees of freedom to actively modify the dispersion orders of artificial slow-light media.

2. Single resonators

In this section, we study theoretically and experimentally the dispersive properties of single passive or active resonators. The building block we have described, in this paper, is shown in Fig. 1. It consists of a resonator coupled to a bus waveguide with an amplitude coupling coefficient κ. Only one mode is considered both for the access waveguide and for the resonator. n is the effective group index of the mode and L is its round trip length propagation. Thus, the resonance frequencies are separated by the free spectral range (FSR) $\Delta\nu = c/(nL) = 1/\tau_L$ where τ_L is the round trip duration. The resonator mode of amplitude u is excited using an input field E_{in}. The total photon lifetime $\tau/2$ in the resonator is related to the coupling with the waveguide lifetime $\tau_e/2$ by: $1/\tau = 1/\tau_0 + 1/\tau_e$, where $\tau_0/2$ is the intrinsic photon lifetime. The coupling photon lifetime is related to the usual amplitude coupling (κ) and reflection (ρ) coefficients by: $\tau_e = \tau_L \sqrt{|\rho|}/(1 - |\rho|)$ where we have $|\kappa|^2 + |\rho|^2 = 1$. The intrinsic photon lifetime is related to the amplitude round trip attenuation a by: $\tau_0 = \tau_L \sqrt{a}/(1 - a)$, these last expressions are useful to obtain the correspondence between the present model and the coupling matrix approach proposed by A. Yariv [8]. $\tau_0 > 0$ corresponds to optical attenuation whereas $\tau_0 < 0$ corresponds to optical gain. By introducing the resonance angular frequency ω_0 of the resonator mode, we can define the external $Q_e = \omega_0 \tau_e/2$, the intrinsic or unloaded $Q_0 = \omega_0 \tau_0/2$ and the loaded $Q = \omega_0 \tau/2$ Q-factors. The time evolution of u can be obtained using a simple harmonic oscillator model as proposed by H.A. Haus [9]:

$$\frac{\mathrm{d}u}{\mathrm{d}t} = \left(j\omega_0 - \frac{1}{\tau} \right) u(t) + \sqrt{\frac{2}{\tau_e}} E_{in}(t) \tag{1}$$

The waveguide output field E_{out} is related to u by:

$$E_{out}(t) = -E_{in}(t) + \sqrt{\frac{2}{\tau_e}} u(t) \tag{2}$$

Thus, we can define the amplitude transmission of the system by: $y = E_{out}/E_{in} = \sqrt{T} e^{j\phi}$, where T is the power transmission.

2.1. Stationary regime

First, let us consider the stationary regime. Therefore we will assume that: $E_{in}(t) = A \exp(j\omega t)$ where $\omega = \omega_0 + 2\pi\delta$ and δ is the frequency detuning from resonance. It is then straightforward to write the amplitude transfer function:

$$y(\delta) = \frac{1/\tau_e - 1/\tau_0 - 2j\pi\delta}{1/\tau_e + 1/\tau_0 + 2j\pi\delta} \tag{3}$$

The power transmission of the resonator can be deduced by:

$$T(\delta) = \left|y(\delta)\right|^2 = \frac{(1/\tau_e - 1/\tau_0)^2 + 4\pi^2\delta^2}{(1/\tau_e + 1/\tau_0)^2 + 4\pi^2\delta^2} \tag{4}$$

The transmission spectrum has a Lorentzian shape and its full width at half maximum (FWHM) is called $2\delta_{1/2}$ which is related to the overall Q-factor by:

$$Q = \frac{\nu_0}{2\delta_{1/2}} \tag{5}$$

where $\nu_0 = \omega_0/(2\pi)$ is the optical frequency. The transmission at resonance ($\delta = 0$) can be written:

$$T(0) = \left(\frac{\tau_e - \tau_0}{\tau_e + \tau_0}\right)^2 \tag{6}$$

This expression shows that when $\tau_0 = \tau_e$ the transmission at resonance vanishes. This corresponds to the critical coupling regime. One can also define the undercoupling ($\tau_0 < \tau_e$) and the overcoupling ($\tau_0 > \tau_e$) regimes [8]. If $\tau_0 < -\tau_e < 0$ (in this case $1 < a < 1/\rho$), the resonator does not sustain laser oscillations but $T(0) > 1$ and it can be seen as a selective amplifier with a bandwidth equal to $2\delta_{1/2}$ [8]. All these regimes are summarized in Fig. 2(a) which represents the resonant transmission $T(0)$ in dB as a function of $1/\tau_0$ for a given value of τ_e. We would also like to highlight the laser oscillations ($\tau_0 \to -\tau_e$) and the transparency ($\tau_0 \to \infty$) points. From an experimental point of view, the value of Q can be deduced from the measurement of $2\delta_{1/2}$ using Eq. (5). The direct measurement of Q_0 and Q_e from $T(\delta)$ is much more complicated since τ_0 and τ_e play the same role in Eq. (4). The only coupling regime which can be identified using the power transmission is the critical coupling when the transmission at resonance drops to zero, in this case we obtain $Q_e = Q_0 = 2Q$. Still in the stationary regime, we can discuss the dispersive properties of the single resonator. In the case of a monochromatic input wave, the following expressions give $\phi(\delta) = \arg[y(\delta)]$ which corresponds to the phase shift introduced by the resonator:

Amplification $\qquad \tau_0 < -\tau_e$: $\quad \phi(\delta) = -\arctan\left(\dfrac{2\pi\delta\tau_0\tau_e}{\tau_0 - \tau_e}\right) - \arctan\left(\dfrac{2\pi\delta\tau_0\tau_e}{\tau_0 + \tau_e}\right)$ $\qquad\qquad$ (7)

Overcoupling $\qquad \tau_0 > \tau_e$: $\quad \phi(\delta) = -\arctan\left(\dfrac{2\pi\delta\tau_0\tau_e}{\tau_0 - \tau_e}\right) - \arctan\left(\dfrac{2\pi\delta\tau_0\tau_e}{\tau_0 + \tau_e}\right)$ $\qquad\qquad$ (8)

Critical coupling $\qquad \tau_0 = \tau_e$: $\quad \phi(\delta) = \pi + \dfrac{\pi}{2}\dfrac{\delta}{|\delta|} - \arctan(\pi\delta\tau_0)$ $\qquad\qquad$ (9)

Undercoupling $\qquad \tau_0 < \tau_e$: $\quad \phi(\delta) = \pi - \arctan\left(\dfrac{2\pi\delta\tau_0\tau_e}{\tau_0 - \tau_e}\right) - \arctan\left(\dfrac{2\pi\delta\tau_0\tau_e}{\tau_0 + \tau_e}\right)$ $\qquad\qquad$ (10)

The phase shift is dependent on the coupling regime and thus, by measuring $\phi(\delta)$ introduced by the resonator the coupling regime can be unambiguously determined [10]. Since we are interested in the dispersion properties of the resonator we also give here the expression of the group delay τ_g calculated using the following definition:

$$\tau_g(\delta) = \frac{\partial\phi}{\partial\omega} = \frac{1}{2\pi}\frac{\partial\phi}{\partial\delta} \tag{11}$$

which gives using the previous notations (excluding the case where we have simultaneously $\delta = 0$ and $\tau_e = \tau_0$):

$$\tau_g(\delta) = -\tau_e\tau_0\left[\frac{\tau_0 - \tau_e}{(\tau_0 - \tau_e)^2 + (2\pi\delta\tau_0\tau_e)^2} + \frac{\tau_0 + \tau_e}{(\tau_0 + \tau_e)^2 + (2\pi\delta\tau_0\tau_e)^2}\right] \tag{12}$$

(a) Transmission at resonance $T(\delta = 0)$

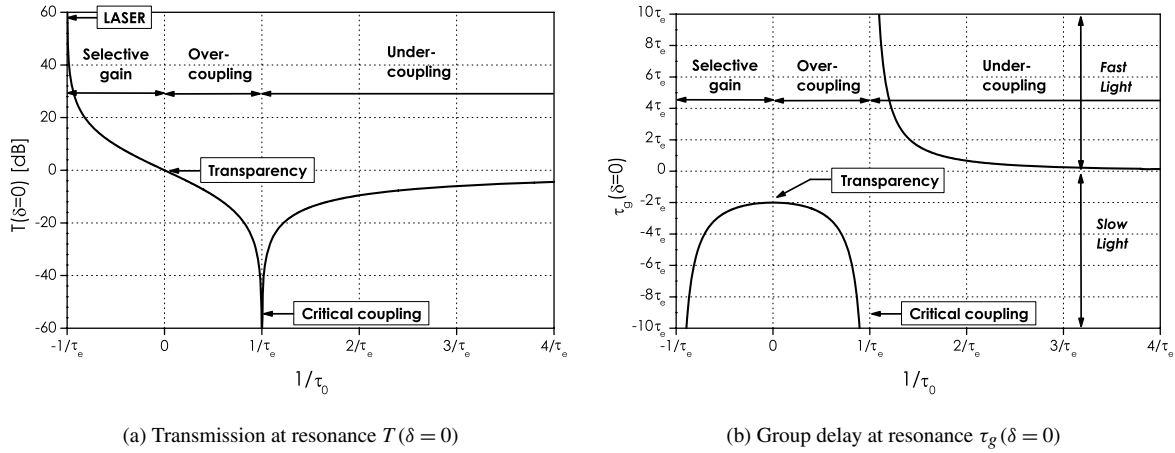(b) Group delay at resonance $\tau_g(\delta = 0)$

Fig. 2. Transmission at resonance $T(\delta = 0)$ in dB and resonant group delay $\tau_g(\delta = 0)$ as a function of $1/\tau_0$ for the different regimes: undercoupling, critical coupling, overcoupling, selective amplification. We also highlight the transparency of the resonator and the laser threshold. In (b) we also show the slow- and fast-light regimes.

As it has been previously done for the transmission, we can calculate the group delay introduced by the structure at resonance:

$$\tau_g(0) = -2 \frac{\tau_e \tau_0^2}{\tau_0^2 - \tau_e^2} \tag{13}$$

In Fig. 2(b), we represent $\tau_g(0)$ for the different coupling regime, as it has been done in Ref. [11]. Unlike the transmission, the resonant group delay strongly depends on the coupling properties: for a given Q, a negative delay (slow-light) is obtained for overcoupling whereas a positive delay (fast-light) is observed for the undercoupling case. As a conclusion, the dispersive properties of a single resonator strongly depend on the coupling properties which cannot be elucidated using the transmission spectrum. Thus, phase or pulse propagation measurements [10,12] must be carried out in order to fully characterize simple devices such as side coupled single resonators.

2.2. Dynamic behavior

We will now consider a linear temporal variation of the excitation frequency ω and we consider that $E_{in}(t) = A \exp[j\theta(t)]$ where $\theta(t) = \omega(t) \cdot t$ with $\omega(t) = \omega_i + \Omega t/(2T_S)$, thus the instantaneous frequency is given by:

$$\frac{\mathrm{d}\theta}{\mathrm{d}t} = \omega_i + \frac{\Omega}{T_S} t \tag{14}$$

At the beginning of the angular frequency sweeping ($t = 0$) the resonator is excited with a stationary wave of frequency ω_i and Ω is the total angular frequency range scanned during the duration T_S. The integration of Eq. (1) leads to:

$$u(t) = \sqrt{\frac{2}{\tau_e}} A \exp\left(j\omega_0 t - \frac{t}{\tau} \right) \left[f(t) - f(0) + \frac{1}{j(\omega_i - \omega_0) + 1/\tau} \right] \tag{15}$$

with:

$$f(t) - f(0) = \int_0^t \exp\left[j\theta(t') + \left(\frac{1}{\tau} - j\omega_0 \right) t' \right] \mathrm{d}t' \tag{16}$$

which can be expressed using the complex error function $\mathrm{erf}(z)$ with $z \in \mathbb{C}$:

$$f(t) = -\sqrt{\frac{j\pi}{2V_S}} \exp\left[\frac{-j(2\pi\delta_i - j/\tau)^2}{2V_S} \right] \mathrm{erf}\left(\frac{j/\tau - 2\pi\delta_i - V_S t}{\sqrt{2jV_S}} \right) \tag{17}$$

(a) Critical coupling ($\tau_0 = \tau_e$)

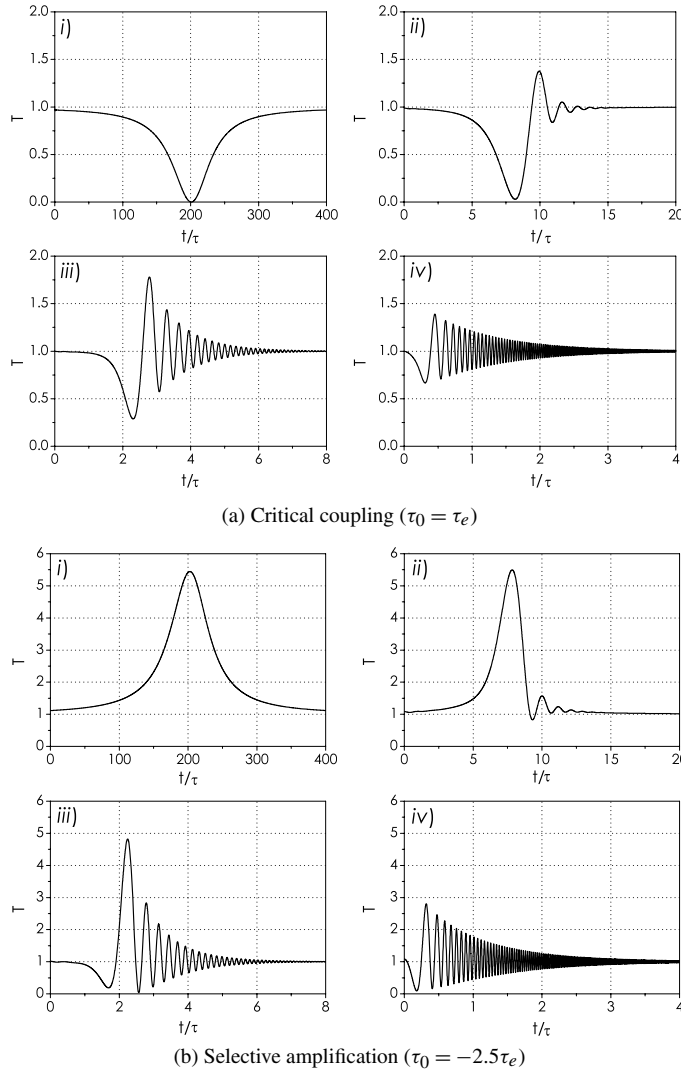(b) Selective amplification ($\tau_0 = -2.5\tau_e$)

Fig. 3. Theoretical transmission as a function of t/τ in the cases of a critically coupled resonator and a selective amplifier for different sweeping speeds. i) $\widetilde{V}_S = 0.0075\widetilde{V}_0$, ii) $\widetilde{V}_S = 0.3\widetilde{V}_0$, iii) $\widetilde{V}_S = 3\widetilde{V}_0$ and iv) $\widetilde{V}_S = 30\widetilde{V}_0$ where $\widetilde{V}_0 = 2/(\pi\tau^2)$.

where we define: $2\pi\delta_i = \omega_i - \omega_0$ as the initial detuning and $V_S = \Omega/T_S$ or $\widetilde{V}_S = \Omega/(2\pi T_S)$ as the frequency sweeping speed. Using Eqs. (2), (15) and (17), it is possible to analytically obtain the time dependent transmission $T(t)$ of the resonator. In Fig. 3(a), we represent the transmission as a function of t/τ in the case of a critically coupled resonator for different sweeping speeds normalized for $\widetilde{V}_0 = 2/(\pi\tau^2)$ which is calculated assuming $\Omega/(2\pi) = 2\delta_{1/2} = 1/(\pi\tau)$ for a duration equal to the photon lifetime $T_S = \tau/2$. For a low sweeping speed ($0.0075\widetilde{V}_0$), we are almost in the stationary regime and we obtain a Lorentzian profile for the transmission. For higher sweeping speeds, the transmission is really different from the stationary response and we can obtain the ringing phenomenon already discussed by several authors [13–15]. Note that this phenomenon is more pronounced when the sweeping speed increases. A similar effect has been observed in semiconductor photonic crystal active structures [16]. In this system the refractive index of the structure can be dynamically shift using a pump signal via the nonlinear dispersion. For the probe located at the edge of a photonic band, the resonant wavelength is shifted and some oscillations appear in its reflection spectrum. Ringing phenomenon also occurs in the case of resonant amplifiers ($\tau_0 < -\tau_e$). Fig. 3(b) represents the transmission as a function of t/τ in the case of selective amplification (here $\tau_0 = -2.5\tau_e$). For low sweeping speed, the transmission spectrum has a Lorentzian profile and provides a maximal gain value around 5.4. For higher sweeping rates, ringing appears and the maximal visible gain value decreases. The inspection of Eqs. (15) and (17) reveals that unlike the

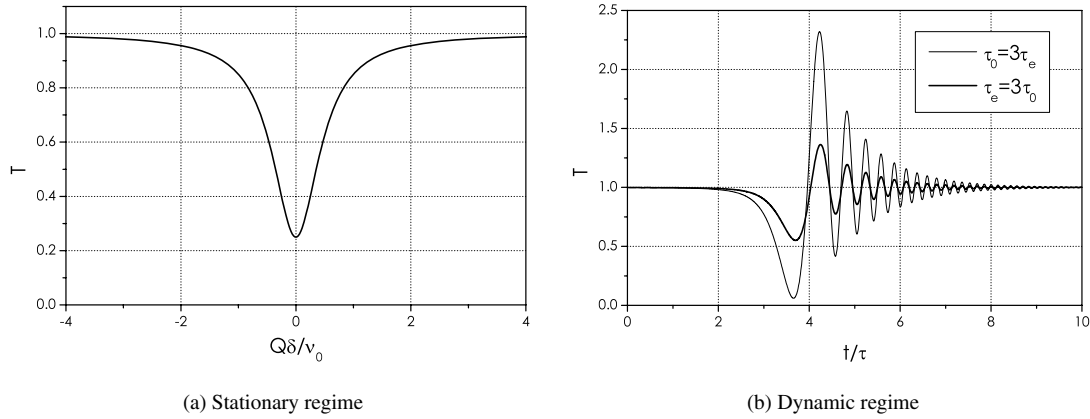(a) Stationary regime (b) Dynamic regime

Fig. 4. (a) Transmission in the stationary case as a function of the normalized detuning in the case of $\tau_0 = 3\tau_e$ and $\tau_e = 3\tau_0$. The responses for the two configurations are exactly superimposed. (b) Transmission as a function of time in the identical two cases with $\widetilde{V}_S = 2.25\widetilde{V}_0$. Note that the two responses are totally different.

stationary case, τ_e and τ_0 no longer play the same role. For a given value of τ, Fig. 4(a) is the stationary response for overcoupled or undercoupled resonators with $\tau_0 = 3\tau_e$ and $\tau_e = 3\tau_0$ respectively whereas Fig. 4(b) represents the transmission for the same two sets of parameters when $\widetilde{V}_S = 2.25\widetilde{V}_0$. These two examples show that it is impossible to distinguish two opposite coupling regimes (over or under coupling) in the stationary regime whereas it is possible in the fast input frequency sweeping regime. As a conclusion of this theoretical section, fast sweeping transmission measurements would allow the coupling regime and the dispersive properties of the single resonators to be fully determined without any phase measurement or pulse propagation experiment.

2.3. Single resonator experiments

In this section, we test experimentally that dynamic measurements allow the coupling regime to be determined unambiguously as it has been proposed in the theoretical section. We also apply this method to the measurement of dispersive properties of a WGM resonator and active fiber resonators. Ref. [17] gives more details about the test of the present method. We used a very simple model system which consists of a ring made from a standard SMF 28 fiber and a spliced section of 1100 ppm Er^{3+} doped fiber [18–21]. The fiber ring resonator is coupled to an access fiber using a tunable coupler [22]. Since we can simultaneously tailor the losses and the coupling of the resonator, this model system allows different coupling configurations to be investigated.

2.3.1. Experimental setup and method

Fig. 5(a) represents the active fiber resonator we use in the experiments. The probe signal is a continuously tunable narrow line (≈ 150 kHz) laser diode. In the experiments, we use two different frequency sweepings: a slow scanning $\widetilde{V}_S \approx 0.40$ MHz/μs which allows us to reach the stationary regime and a fast scanning $\widetilde{V}_S = 5$ MHz/μs which allows ringing phenomenon to be observed. The doped fiber section is pumped using a 980 nm laser diode. We have chosen to use an active fiber to explore all the coupling regimes by changing the pumping rate as we will show later. The ring perimeter is approximatively $L = 2.5$ m, its effective group index $n = 1.46$ and the resonant wavelength is set to 1550 nm leading to $\omega_0 = 1.2 \times 10^{15}$ rad s^{-1}. Note that in the slow sweeping regime, the theoretical value of the FSR is used to deduce $\widetilde{V}_S$. Subsequently we can calibrate the abscissa axis in frequency units as usual. The outcoupled signal from the ring is sent to an optical detector and normalized using the off-resonance value. Then, we are able to obtain the experimental temporal variations of the transmission T_{mes} which was compared in the case of the fast scanning experiments to the theoretical value T_{theo} by using the least square method:

$$\sigma^2(\tau_0, \tau_e, V_S) = \sum_{i=1}^{N} \left[T_{mes,i} - T_{theo,i}(\tau_0, \tau_e, V_S) \right]^2 \tag{18}$$

(a) Coupling regime determination   (b) Coupling regime determination
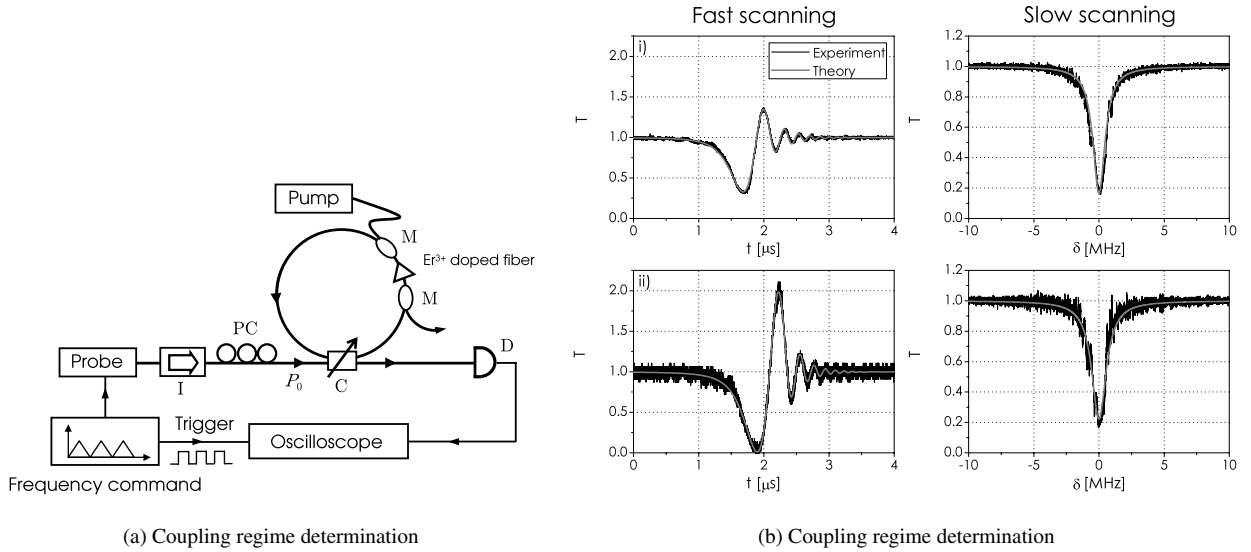
Fig. 5. (a) Setup used to test the experimental method. The resonator consists of SMF 28 fiber with a spliced 50 cm long section of Er^{3+} fiber pumped with a 980 nm laser diode using wavelength multiplexers M. C: tunable coupler, I: optical isolator, PC: polarization controller and D: optical detector. The probe is a tunable 1550 nm laser diode (bandwidth 150 kHz) whose central frequency is linearly swept with a controllable period. P_0 is the optical power of the input signal. The fiber resonator is immersed in a water bath to limit thermal fluctuations. (b) Fast and slow scanning experimental results (black lines) and fitting curves (gray lines) for two combinations of coupling coefficient and pumping rate (4.5 mW and 7 mW) and an input power $P_0 = 1.5$ mW. These two parameters are chosen to switch the role played by τ_0 and τ_e. i) Undercoupling regime: $\tau_0 = 404$ ns, $\tau_e = 958$ ns and $\tau = 284$ ns. ii) Over coupling regime: $\tau_0 = 895$ ns, $\tau_e = 321$ ns and $\tau = 236$ ns. The slow scanning (stationary regime) provides almost the same transmission spectrum.

where N is the number of temporal sampling points. The value of σ^2 is minimized by automatically changing the value of τ_0, τ_e and V_S to obtain the best fit. The knowledge of τ_0 and τ_e allows all the dispersion properties of the single resonator to be precisely determined using Eq. (13) for example.

2.3.2. Direct determination of the coupling regime

We tested the possibility of distinguishing between two opposite coupling regimes for a given overall Q-factor Q. Therefore, we used two sets of coupling and pumping rates giving us nearly the same stationary responses (in the slow scanning regime) as shown in the right column of Fig. 5(b). From these slow scanning experiments we approximatively measured the same $2\delta_{1/2}$ and the same transmission $T(0)$, consequently it is impossible to determine the coupling regime. Using the same conditions, we also performed fast scanning experiments which are presented in the left column of Fig. 5(b). The amplitude of the ringing oscillations reveal the coupling regime and the fits give: a) undercoupling: $\tau_0 = 404$ ns and $\tau_e = 958$ ns; b) overcoupling: $\tau_0 = 895$ ns and $\tau_e = 321$ ns. In the two cases, the global Q-factors deduced from the fast scanning are comparable a) $Q = 1.7 \times 10^8$ and b) $Q = 1.4 \times 10^8$. To check the validity of the measurements of loaded Q-factors obtained with the fast scanning method, we fit the slow scanning results without changing τ_0 and τ_e using Eq. (4). We obtained a good agreement for the two configurations. Note that for higher Q-factors the slow scanning method has several drawbacks such as the need for a high frequency stability laser or the parasitic contributions from nonlinear effects [23]. Moreover, the fast sweeping method does not require $\widetilde{V}_S$ to be calibrated which can be difficult to precisely measure by other techniques.

2.3.3. WGM resonators

We first apply the method to a WGM resonator, by replacing the fiber loop and coupler C of Fig. 5(a) by a MgF_2 disk and its tapered fiber coupler as represented in Fig. 6(a). The disk has a diameter $D = 5.2$ mm, a thickness $e = 0.3$ mm and its polished area has a diameter of about $\rho = 60$ μm. The diameter of the tapered fiber is reduced to 3 μm. In the case of fast sweeping of the probe wavelength, the transmission as a function of time is represented in black in Fig. 6(b). The theoretical fit (gray line) gives $Q_0 = 3.3 \times 10^8$, $Q_e = 2.5 \times 10^9$ which shows that the resonator is undercoupled ($Q_0 < Q_e$). In this case, the method is useful since it directly gives the intrinsic Q-factor Q_0 which
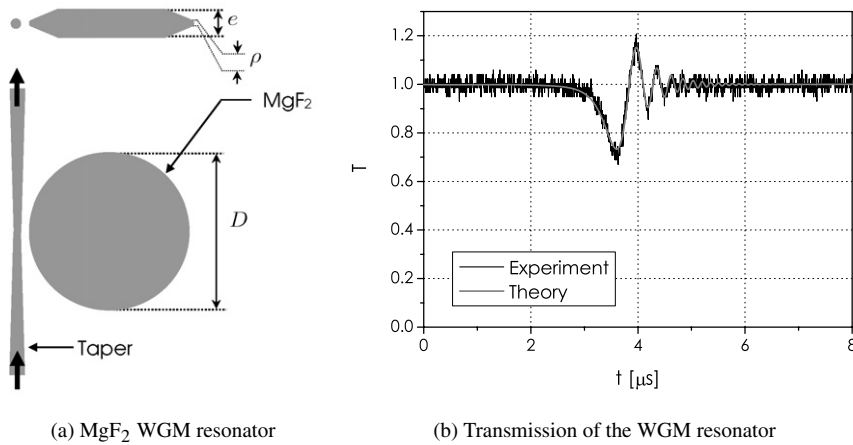
(a) MgF$_2$ WGM resonator   (b) Transmission of the WGM resonator

Fig. 6. (a) Description of the MgF$_2$ WGM resonator with its coupling fiber taper. The minimal diameter of the taper is about 3 μm. $D = 5.2$ mm, $e = 0.7$ mm and the spherical polished part has a diameter $\rho = 60$ μm. (b) Experimental results with the MgF$_2$ WGM resonator (black line). The theoretical fit (gray line) gives: $Q_0 = 3.3 \times 10^8$, $Q_e = 2.5 \times 10^9$.

depends only on the structural characteristics of the WGM resonator. Using Eq. (13), we can also infer the dispersion properties of the group delay at resonance introduced by the WGM resonator $\tau_g(0) = 146$ ns.

2.3.4. Active or amplifying resonators

With the doped fiber resonator already described in Section 2.3.1, it is possible to obtain an almost transparent resonator equivalent to a Gires–Tournois interferometer by adjusting the pumping rate to compensate for all the optical losses. To obtain such a resonator, we tried to obtain a constant transmission in the slow scanning regime. Still to check the validity of our method, we then switched to the fast scanning regime and we obtained the response given in Fig. 7(a). The numerical calculations shown in this figure give: $Q_e = 2.3 \times 10^8$ and $Q_0 = 4.9 \times 10^{14}$. The inferred intrinsic Q-factor is in very good agreement with a lossless resonator and show that the method works well in limit cases. We can also deduce the dispersive properties of this resonator: $\tau_g(0) = -2\tau_e \approx -758$ ns. By increasing the pump power, we can even obtain highly selective amplification [21,24,25]. In our system we have obtained a gain as high as 12.1 dB as presented in Fig. 7(b). In this case, the bandwidth of the selective amplification is 440 kHz. Using Eq. (13), we can also deduce the group delay at resonance: $\tau_g(0) = -900$ ns which shows that this resonator could be used to delay a monochromatic signal by almost 1 μs and to amplify it by more than 10 dB. It is difficult to measure highly selective gain (or very high-Q passive resonators) in the stationary regime since the bandwidth is very narrow. The sweeping rate must be very low to avoid ringing whereas when taking into account the ringing phenomenon it is possible to infer the characteristics of the amplifier. Moreover, one of the main limitations of the stationary method comes from the laser probe linewidth which must be narrower than the resonator linewidth. This limitation can be circumvented in the dynamic regime using high sweeping speeds [26]. All the analysis presented in this paper, were obtained under assumption of linear regime, we assume that there is neither absorption nor gain saturation. For higher gains or higher signal powers the gain or absorption saturation would be taken into account in Eq. (1). The slight discrepancy between the experimental results and the theoretical fit of Fig. 7(b) may come from the fact we have limited our calculations to the linear regime. If absorption or gain saturation have induced significant nonlinear dispersion, we would have observed dynamic bistable profiles. This effect could also be easily taken into account in the model [27]. We also neglect the dynamic behavior of the atomic medium since Er^{3+} characteristics lifetimes are about 10 ms which is much longer than the typical photon lifetimes of our systems. In this case we can assume that the populations of the gain medium are "frozen" during the observation duration [16].

3. Coupled-active-resonator-induced transparency

In the previous section, we analyzed in detail the properties of a single resonator. We have shown that the transmission (or gain) and dispersion are totally determined by the values of τ_e and τ_0. In other words, it is possible to obtain all the combinations of gain and delay by changing the values of the coupling coefficients and adjusting the
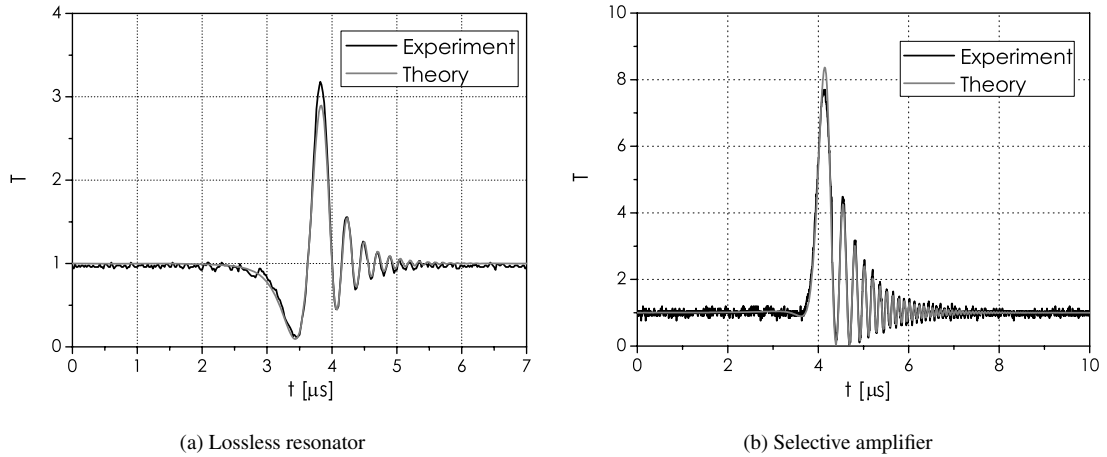
Fig. 7. (a) Experimental results for $P_0 = 1.5$ mW with the fiber resonator for a pumping rate of 7.8 mW. The theoretical fit (gray line) gives: $\tau_0 = 818$ ms, $\tau_e = 379$ ns and thus a resonant transmission of $T(0) \approx 1$, the resonator is equivalent to a Gires–Tournois interferometer. (b) Experimental results for $P_0 = 1.5$ mW with the fiber resonator under high pumping (22.1 mW). The theoretical fit (gray line) gives: $\tau_0 = -476$ ns, $\tau_e = 287$ ns, then $T(0) = 16.3$ (or $T(0) = 12.1$ dB) in a frequency bandwidth $2\delta_{1/2} = 440$ kHz.

optical losses. For example, if one want to obtain a transparent ($T = 1$) delay line the optical losses must be canceled and then $\tau_g(0) = -2\tau_e$. In many applications, the delay line must be tunable. In the present situation, by changing the coupling of the resonator (and thus τ_e) all the group delay values would be reachable. Unfortunately, in a lot of configurations the coupling can be only changed by mechanical means. Moreover, the coupling of integrated devices is really difficult to actively change. Consequently, it would be more convenient that the dispersive properties of the resonator were dependent on τ_0. In this section, we will show that the coupling of two active resonators allows to obtain such transparent tunable delay line. It has already been shown that by coupling two passive resonators one can obtain a classical counterpart of EIT referenced as coupled-resonator-induced transparency (CRIT) [28–36]. The resonator coupling creates a resonance frequencies split (analogous to Rabi splitting in EIT) which cancels the unavoidable absorption of lossy single resonators [29,31].

3.1. Theoretical model

First, we will recall the basic theoretical method based on coupled mode theory for the description of linear properties of two coupled ring resonators [31]. Note that, in the previous section, we used the H.A. Haus model and thus assumed a time dependence in $\exp(j\omega t)$. In this section, since we deal with stationary calculations we have chosen an opposite time dependence which only changes the sign of the group delay. Fig. 8 schematically represents the configuration consisting of two coupled ring resonators allowing the observation of CRIT. The two ring fiber resonators (of total lengths L_1 and L_2) are coupled using a 2×2 coupler C_1. For the sake of clarity and without loss of generality, we will consider that the coupler C_1 is located at exactly $L_2/2$ from coupler C_2 which allows loop 2 and the access fiber to be coupled. Couplers C_i with $i \in \{1, 2\}$ are characterized by a 2×2 matrix [8]:

$$C_i = \begin{bmatrix} \rho_i & j\kappa_i \\ j\kappa_i & \rho_i \end{bmatrix}, \quad i \in \{1, 2\} \tag{19}$$

where the coupling coefficients ρ_i and κ_i are related by: $\gamma_i = \rho_i^2 + \kappa_i^2$ with $\gamma_i \leqslant 1$. In this paper we deal with single mode monochromatic fields of angular frequency ω. The field envelopes E_5 and E_2 after C_1 are related to the envelopes E_4 and E_1 before C_1 by:

$$\begin{bmatrix} E_5 \\ E_2 \end{bmatrix} = C_1 \begin{bmatrix} E_4 \\ E_1 \end{bmatrix} \tag{20}$$

During its round-trip in loop 1, E_5 undergoes an attenuation a_1 and a phase shift $\phi_1 = n\omega L_1/c$ where n is the effective refractive index of the fiber, thus the field envelope E_4 reads:
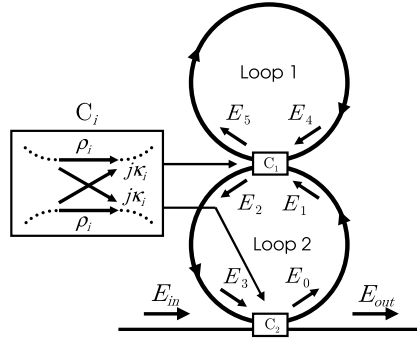
Fig. 8. The coupled resonators system consists of two fiber loops (with effective refractive group index n) of length L_1 and L_2 coupled by a 2×2 coupler C_1. The system is coupled to a bus fiber via the coupler C_2. The input and output fields are E_{in} and E_{out}. E_i with $i \in [0, 5]$ are the field envelope values at several points inside the coupled resonator system.

$$E_4 = a_1 E_5 e^{j\phi_1} \tag{21}$$

Using Eqs. (20) and (21), we can write the expression of the transmission coefficient t_1 associated with loop 1:

$$y_1 = \frac{E_2}{E_1} = \frac{\rho_1 - \gamma_1 a_1 e^{j\phi_1}}{1 - \rho_1 a_1 e^{j\phi_1}} \tag{22}$$

The same method applied for loop 2, the field envelopes E_0, E_3, E_{in} and E_{out} are related by:

$$\begin{bmatrix} E_{out} \\ E_0 \end{bmatrix} = \mathcal{C}_2 \begin{bmatrix} E_{in} \\ E_3 \end{bmatrix} \tag{23}$$

We call a_2 and $\phi_2 = n\omega L_2/c$ the attenuation and the phase shift in loop 2, then we have:

$$E_i = \sqrt{a_2} E_{i-1} e^{j\phi_2/2}, \quad i \in \{1, 3\} \tag{24}$$

By combining Eqs. (23) and (24), we obtain the amplitude transmission y of the whole system:

$$y = \frac{\rho_2 - \gamma_2 a_2 y_1 e^{j\phi_2}}{1 - \rho_2 a_2 y_1 e^{j\phi_2}} \tag{25}$$

which can be explicitly written using Eq. (22):

$$y = \sqrt{T} e^{j\phi} = \frac{\rho_2 - \rho_1 \rho_2 a_1 e^{j\phi_1} - \gamma_2 \rho_1 a_2 e^{j\phi_2} + \gamma_1 \gamma_2 a_1 a_2 e^{j(\phi_1+\phi_2)}}{1 - \rho_1 a_1 e^{j\phi_1} - \rho_1 \rho_2 a_2 e^{j\phi_2} + \gamma_1 \rho_2 a_1 a_2 e^{j(\phi_1+\phi_2)}} \tag{26}$$

The dispersion properties of the coupled resonator system are quantified by the high dispersion orders $\beta_p = \partial^p \phi / \partial \omega^p$ $p > 1$ (note that for $p = 1$ we obtain the group delay already defined).

3.2. Coupled-resonator-induced transparency

A convenient choice of coupling coefficients ρ_i and optical attenuations a_i where $i \in \{1, 2\}$ allows to obtain different coherent optical effects. In this paper, we will only deal with CRIT in the case of coupled optical fiber rings. We consider here that $L_1 = L_2 = L$ (so $\phi_1 = \phi_2 = \varphi$) and $\gamma_1 = \gamma_2 = 1$. Let us also assume no material dispersion and that the two rings have a common resonance frequency ω_0. We note δ the frequency detuning from the resonance frequency: $\omega = \omega_0 + 2\pi\delta$. Fig. 9(a) represents in solid line the whole absorption of the system $A = 1 - T$ as a function of δ in a configuration of CRIT ($a_1 = 0.9995$, $a_2 = 0.76$, $\rho_1 = 0.995$ and $\rho_2 = 0.95$). We also represent in Fig. 9(a) the total absorption A for resonator 2 alone (dash–dot line). We can note that the coupling of resonator 1 induces a splitting of the large absorption resonance of resonator 2 in two absorption peaks and that a narrow transparency window appears between the split resonances. The resonance splitting can be found as follows. We first write the field envelope value inside resonator 2:
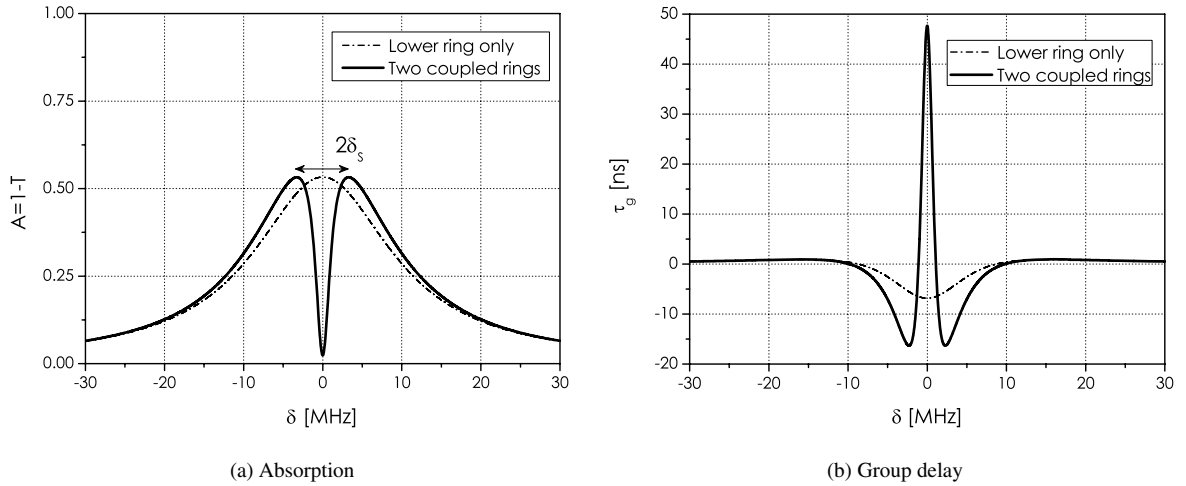
(a) Absorption

(b) Group delay

Fig. 9. Coupled resonator system with $a_1 = 0.9995$, $\rho_1 = 0.995$, $a_2 = 0.76$, $\rho_2 = 0.95$, $L_1 = L_2 = L \approx 1$ m, $\lambda_0 = 1.55$ μm and $n = 1.46$. (a) Absorption $A = 1 - T$ as a function of the detuning δ. We also represent the absorption A for the lower resonator (resonator 2). $2\delta_S$ is the frequency split coming from the coupling of the two resonators. (b) Dispersion properties of the coupled resonators. We also recall the group delay of the lower resonator.

$$\frac{E_0}{E_{in}} = \frac{j\kappa_2}{1 - \rho_2 a_2 y_1 e^{j\varphi}} \tag{27}$$

We note $D = 1 - \rho_2 a_2 y_1 e^{j\varphi}$ the denominator of Eq. (27). For the new resonance frequencies the field inside resonator 2 is maximal and then $|D|$ is minimal. If we note δ_S the value of the detuning δ of the split resonance frequencies, we have:

$$\left.\frac{\partial |D|}{\partial \delta}\right|_{\delta_S} = 0 \tag{28}$$

Assuming that $a_1 \approx 1$ and using a first-order development in $1 - \rho_1$ we obtain the two values of the detuning for the split resonances:

$$\delta_S = \pm \frac{1}{\pi \tau_L} \sqrt{\frac{1 - \rho_1}{2}} \tag{29}$$

The solid line in Fig. 9(b) plots the group delay τ_g as a function of δ for the coupled resonators in the configuration of CRIT. As it was the case for absorption A, we also represented in dash–dot line dispersion properties of the lower resonator alone. The coupling between the two resonators induces a sharp positive phase variation which leads to a positive group delay. The CRIT configuration allows both a high transmission and a large delay to be obtained simultaneously which constitute crucial properties for optical delay line [30,31]. If we choose $\rho_1 = a_1$, the transmission at resonance is $T(\delta = 0) = \rho_2^2$ and independent on a_2. Conversely, the resonant group delay depends linearly on a_2:

$$\tau_g(0) = a_2 \frac{\rho_1(1 - \rho_2^2)}{\rho_2(1 - \rho_1^2)} \tau_L \tag{30}$$

This configuration is potentially interesting for applications since the coupled resonator system acts as an almost transparent delay line ($\rho_2 \approx 1$) whose group delay is changed by varying a_2. Eq. (30) also shows that coupling coefficients must be chosen as $1 - \rho_1 \ll 1 - \rho_2$ in order to obtain a large delay. This could be done using active resonators whose pumping rate is controlled. The main differences with the single resonator are: i) the delay is changed without modifying the coupling rates, ii) the optical losses do not change the transmission value. Under the same assumption that those made to obtain Eq. (30) we can also calculate the FWHM of the transmission of the two resonator system:

$$2\delta_{1/2} = \frac{1 - \rho_1^2}{\pi \tau_L \rho_1(\rho_2 a_2 - \rho_1)} \tag{31}$$
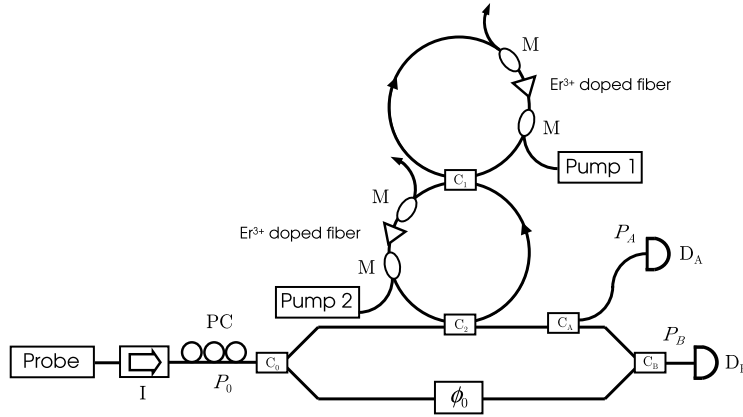
Fig. 10. The experimental setup is composed of two coupled active fiber loops inserted in one arm of a Mach–Zehnder fiber interferometer. C_1 is a 99%/1% coupler, C_2 is a 90%/10% coupler whereas C_0, C_A and C_B are 3 dB couplers. PC is a polarization controller and I is an optical isolator. M are wavelength division multiplexers allowing the insertion of the 980 nm pump lasers 1 and 2 into the two 30 cm long Er^{3+} doped fiber sections. P_0 is the optical power entering the interferometer, P_A and P_B are respectively the incident optical powers on detectors D_A and D_B. The length of the lower arm of the interferometer is chosen to cancel the phase dispersion due to chromatic dispersion of SMF 28, it introduces a static phase shift ϕ_0. The probe is an external-cavity laser diode with a bandwidth of 150 kHz tunable around 1550 nm. To limit thermal fluctuations, we immersed the coupled rings in a water bath.

which leads to a bandwidth-delay product:

$$2\delta_{1/2}\tau_g(0) = \frac{2(1-\rho_2)a_2}{\pi(1-\rho_2 a_2)} \leqslant \frac{2}{\pi} \tag{32}$$

where $2/\pi$ is the bandwidth-delay product for a one resonator all-pass filter [37]. In this configuration the bandwidth-delay product is smaller than for a single lossless resonator [37] but the group delay is controllable.

3.3. Experimental results

In this section, we propose an experimental demonstration of the tunable transparent delay line made of a coupled resonator system. As it was the case for the single resonator experimental study we used Er^{3+} doped fiber allowing us to actively and independently control the values of a_1 and a_2. The experimental arrangement is described in Fig. 10. We used telecom single mode fiber (SMF 28) loops with spliced sections of 1100 ppm Er^{3+} doped fiber. The loops are pumped in opposite directions individually by two 980 nm pump laser diodes. The loop 1 is pumped using laser 1 whose power is 8.6 mW. The probe signal is delivered by the tunable 1550 nm laser diode already described, P_0 is still the optical input power. In order to measure the total phase shift $\phi(\delta)$ (and thus the group delay), the coupled resonators are also coupled to one arm of a Mach–Zehnder fiber interferometer using two 3 dB couplers C_0 and C_B. This technique has already been used to measure the dispersion of slow-light systems such as EIT media [38,39], single passive fiber resonators [22] or atomic vapor [40]. Another 3 dB coupler C_A is used to obtain a direct measurement of the transmission T. It is straightforward to write the expressions of optical powers inside the upper arm:

$$P_A(\delta) = P_0\rho_0^2 T(\delta)\rho_A^2 \tag{33}$$

and at the output of the interferometer $P_B(\delta)$:

$$P_B(\delta) = P_0\{X^2(\delta) + X_0^2 + 2X(\delta)X_0 \cos[\phi(\delta) - \phi_0]\} \tag{34}$$

where $X(\delta) = \sqrt{T(\delta)}\rho_0\kappa_A\rho_B$. $X_0 = \kappa_0\kappa_B$ and ϕ_0 is the global static phase shift between the two arms. We carefully measured several experimental parameters: i) the input power $P_0 = 2.62$ mW, ii) the coupling coefficients of C_0, C_2, C_A and C_B, iii) optical losses of each component which will be taken into account in the values of coupling coefficients and iv) the sensitivities of detectors D_A and D_B. By scanning the probe wavelength and by simultaneously measuring the optical power values $P_A(\delta)$ and $P_B(\delta)$, we firstly deduce the transmission $T(\delta)$ using Eq. (33), and then the whole phase shift $\phi(\delta)$ using Eq. (34):
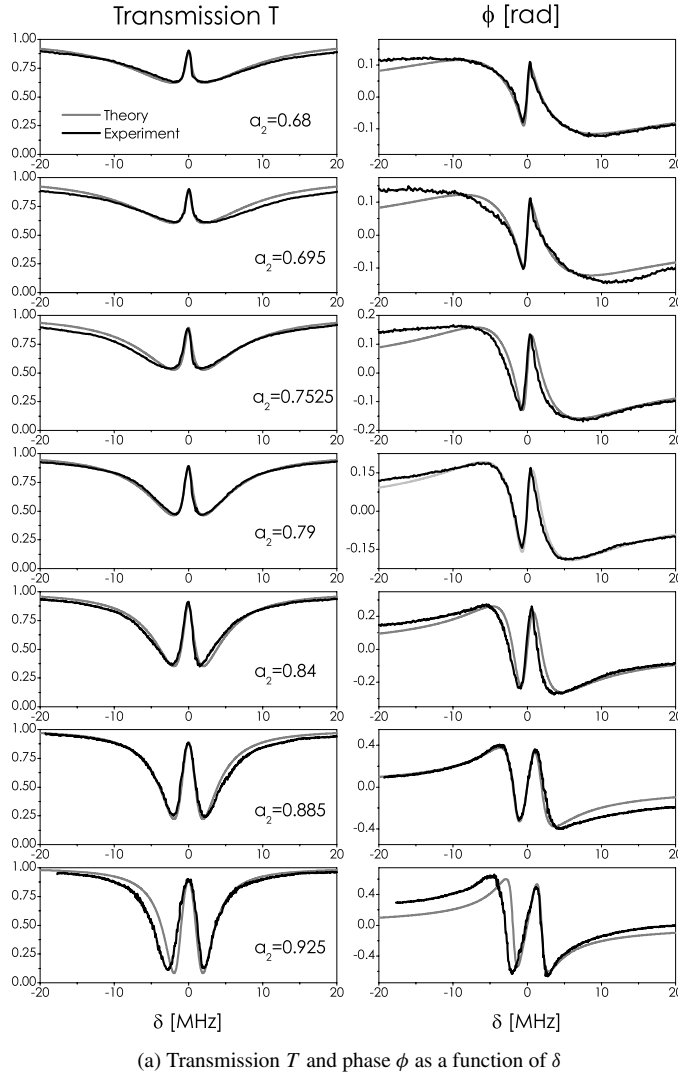
(a) Transmission T and phase ϕ as a function of δ

Fig. 11. In both figures black curves are experimental measurements and gray curves are theoretical calculations. The only parameter which is changed in each row is the value of the attenuation a_2 in loop 2. For the group delay, the experimental curves are deduced by numerically calculating the first derivative of the experimental values. For the group delay dispersion β_2 we only give the theoretical values. We give the inferred values of a_2 in the left columns. From the top to the bottom, the pump 2 power values are: 1.7 µW, 150 µW, 850 µW, 1.62 mW, 2.24 mW, 4.52 mW, 7.77 mW.

$$\phi(\delta) = \phi_0 + \arccos\left[\frac{P_B(\delta)/P_0 - X^2(\delta) - X_0^2}{2X(\delta)X_0}\right] \tag{35}$$

It is then possible to infer the value of $\tau_g(\delta)$ by differentiating $\phi(\delta)$. In order to reduce the noise impact on the numerical evaluation of $\tau_g(\delta)$, we smoothed $P_A(\delta)$, $P_B(\delta)$ and $\phi(\delta)$ using successively FFT and Savitzky–Golay filters. The probe wavelength is scanned over a spectral range of about 5 GHz in order to find a coincident resonant angular frequency ω_0 for the two loops. Black curves of Fig. 11(a) represent the experimental transmission T (left column) and the phase shift ϕ (right column) as a function of the detuning δ for seven loop 2 pumping rates. The zero detuning ($\delta = 0$) is centered at the transmission maximum. The mean value of $\phi(\delta)$ is subtracted to avoid ϕ_0 measurement. These results are fitted (gray curves) using modulus and argument of Eq. (26). To perform theoretical calculations, we independently measured the lengths of the fibers: $L_1 = 1.205$ m, $L_2 = 1.410$ m and we assumed that doped fiber sections have roughly the same effective group index dispersion as SMF 28 fiber (i.e. we considered that $\phi_i(\delta) = n(\delta)\omega L_i/c$ where $i \in \{1, 2\}$ and $n(\delta)$ is the effective group index of standard single mode fiber). We
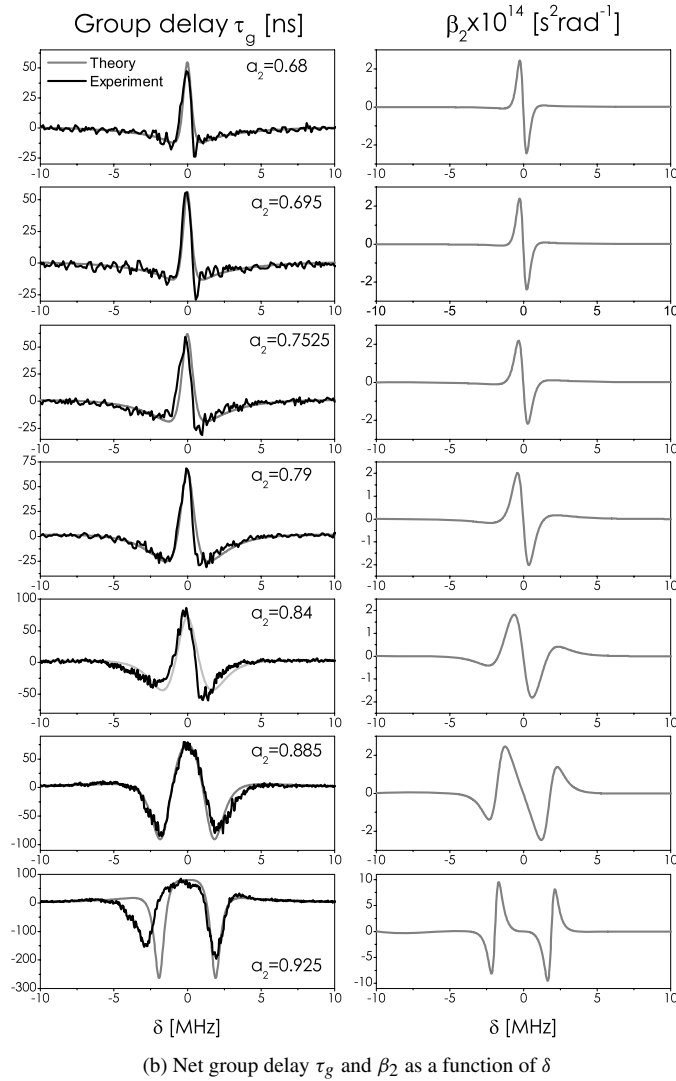
(b) Net group delay τ_g and β_2 as a function of δ

Fig. 11. (*continued*)

also measured the value of the coupling coefficient of C$_2$: $\kappa_2^2 = 8.7\%$, the only fitting parameters are i) the value of the coupling coefficient of C$_1$: $\kappa_1^2 = 0.6\%$, ii) $a_1 = 0.996$ and iii) a_2 which is changed for each pumping rate. We considered lossless couplers. For an increase in the pumping rate of the lower ring, the off-resonance absorption increases. This confirms the coherent behavior of the optical phenomenon observed and that the effect of spontaneous emission is negligible. We have also checked that spontaneous emission does not introduce too much incoherent noise by measuring the response of the system without probe signal. The amplitude of the phase-shift increases when we increase the value of a_2. In this case, we numerically checked that for $0.7 \leqslant |\phi_0| \leqslant \pi - 0.7$, the effect of ϕ_0 is only reduced to a phase offset or a sign reversal in the phase shift $\phi(\delta)$. This justifies the use of Eq. (35). The experimental data and theoretical calculations show a good agreement for several pumping rates of loop 2. We have chosen a constant value for the pumping rate of the first loop (which corresponds to a fixed value for a_1) in order to fulfill the hypothesis made to obtain Eq. (30). From the measurement of the dispersion, it is possible to infer the group delay. In the left column of Fig. 11(b), we have represented in black the group delay τ_g obtained by numerical differentiation of the experimental values of $\phi(\delta)$ as a function of the detuning δ. These results are compared to the first derivatives of the theoretical calculation of $\phi(\delta)$ (see gray curves in the left column of Fig. 11(b)). In the right column of Fig. 11(b), we added the theoretical values of $\beta_2(\delta)$ which vanishes when $\delta = 0$ due to the parity of $\tau_g(\delta)$.
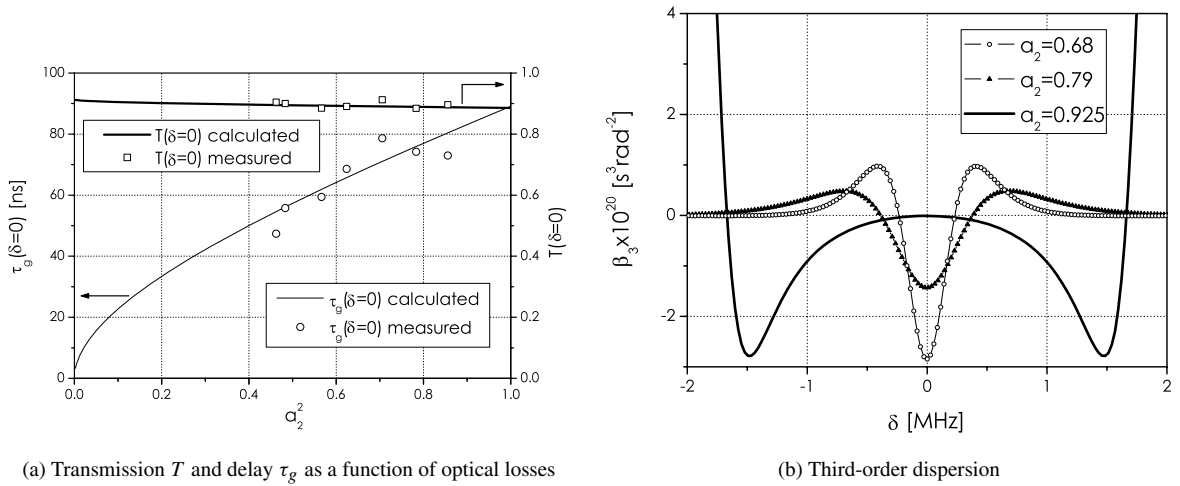
(a) Transmission T and delay τ_g as a function of optical losses

(b) Third-order dispersion

Fig. 12. (a) The thin line (left scale) is the calculation of the group delay at resonance $\tau_g(\delta = 0)$ as a function of optical power attenuation a_2^2 of loop 2. The open circles are the experimental evaluation of $\tau_g(\delta = 0)$ deduced from Fig. 11(b). The thick line (right scale) is the theoretical value of the transmission at resonance $T(\delta = 0)$ as a function of a_2^2. The open squares are the experimental measurements of $T(\delta = 0)$. (b) Theoretical calculations of the third-order dispersion $\beta_3(\delta)$ for three values of a_2 in the case of our experimental system.

First, we can note that when the pumping rate of the lower resonator increases the resonant group delay also increases without modifications of the resonant transmission as it has been theoretically proposed. We summarized the result in Fig. 12(a) where we plotted both the resonant group delay and the resonant transmission as a function of the optical attenuation a_2^2. Second, as the pumping rate increases we can also observe that the group delay spectrum broadens and flattens. This enlarges the spectral range where the group delay dispersion β_2 vanishes [see Fig. 11(b)]. This feature is associated with simultaneous canceling of the third-order dispersion. To underline this effect, we calculated and represented in Fig. 12(b) the third-order dispersion as a function of δ for three values of a_2. For the particular value of $a_2 = 0.925$, β_3 vanishes at resonance. This show that, for a given system of coupled resonators, the active feature allows its dispersion properties to be tuned using external parameters such as the pumping rate.

4. Conclusion

We have described in detail the dispersion properties of active single and coupled resonators. For single resonators, we have proposed a simple experimental protocol used in the time domain to obtain all their characteristics. We experimentally applied the method to Er^{3+} doped fiber ring resonator and to WGM resonators. We also studied Er^{3+} doped coupled fiber ring resonators in the stationary regime. We have experimentally demonstrated that the active behavior of the resonators allows the group delay and the high dispersion orders to be tailored keeping the system transparent. These artificial media may find some applications in different domains. For example, high Q-factor optical resonators are of interest for microwave generation [41]. In microwave photonics, optical resonators can be used as filters or delay line in optoelectronic oscillators [41]. In this last case, the knowledge of the dispersive properties of the resonator may be crucial. In this purpose, we can also notice that the case of selective amplification is interesting since it allows both an amplification and a delay of the optical signal. From another point of view, the experimental method of Q-factor measurement shown in this paper could have important applications in integrated optics since it gives the value of the intrinsic Q-factor of the resonators (without its coupler) in one set of measurement. The use of active coupled resonators could be of interest for tunable delay lines in the microwave domain [41,42]. We have showed that the active feature of coupled resonators acts as a supplementary external parameter to tailor the different dispersion orders of coupled resonators. It has already been proposed to flatten the group delay dispersion in order to cumulate delay in coupled resonator by engineering the coupling coefficients [43,37,44]. Using active device, it could be possible to adjust the dispersion after fabrication. These results could be useful for predicting of the behavior of active coupled microresonators used in the integration of photonic functions [45–47], in this case the dynamic of the gain will have to be considered [16]. Finally, coupled resonators could be used to increase the sensibility of

interferometers [48,49] in particular, it could be envisaged to use CRIT systems to increase the sensitivity of optical gyroscopes [50,51].

References

 [1] S.E. Harris, J.E. Field, A. Imamoğlu, Phys. Rev. Lett. 64 (1990) 1107–1110.
 [2] L.V. Hau, S.E. Harris, Z. Dutton, C.H. Behroozi, Nature (London) 397 (1999) 594–598.
 [3] M.S. Bigelow, N.N. Lepeshkin, R.W. Boyd, Phys. Rev. Lett. 90 (2003) 113903.
 [4] M. Herráez, K.Y. Song, L. Thévenaz, Appl. Phys. Lett. 87 (2005) 081113.
 [5] G. Lenz, B.J. Eggleton, C.K. Madsen, R.E. Slusher, IEEE J. Quantum Electron. 37 (2001) 525–532.
 [6] T. Baba, Nat. Photon. 2 (2008) 465–473.
 [7] F. Xia, L. Sekaric, Y. Vlasov, Nat. Photon. 1 (2007) 65–71.
 [8] A. Yariv, Electron. Lett. 36 (2001) 321–322.
 [9] H.A. Haus, Waves and Fields in Optoelectronics, Prentice-Hall, 1984.
[10] B.J.J. Slagmolen, M.B. Gray, K.G. Baigent, D.E. McClelland, Appl. Opt. 39 (2000) 3638–3643.
[11] S. Minin, M.R. Fisher, S.L. Chuang, Appl. Phys. Lett. 84 (2004) 3238–3240.
[12] G.S. Pandian, F.E. Seraji, IEE Proc. 138 (1991) 235–239.
[13] H.J. Schmitt, H. Zimmer, IEEE Trans. Microwave Theory Tech. 14 (1966) 206–207.
[14] Z.K. Ioannidis, P.M. Radmore, I.P. Giles, Opt. Lett. 13 (1988) 422–424.
[15] J. Poirson, F. Bretenaker, M. Vallet, A. Le Floch, J. Opt. Soc. Am. B 14 (1997) 2811–2817.
[16] A.M. Yacomotti, F. Raineri, C. Cojocaru, P. Monnier, J.A. Levenson, R. Raj, Phys. Rev. Lett. 96 (2006) 093901.
[17] Y. Dumeige, S. Trebaol, L. Ghisa, T.K.N. Nguyen, H. Tavernier, P. Féron, J. Opt. Soc. Am. B 25 (2008) 2073–2080.
[18] L.F. Stokes, M. Chodorow, H.J. Shaw, Opt. Lett. 7 (1982) 288–290.
[19] B. Crosignani, A. Yariv, P. Di Porto, Opt. Lett. 11 (1986) 251–253.
[20] J.T. Kringlebotn, P.R. Morkel, C.N. Pannell, D.N. Payne, R.I. Lamimg, Electron. Lett. 28 (1992) 201–202.
[21] J.M. Choi, R.K. Lee, A. Yariv, Opt. Lett. 26 (2001) 1236–1238.
[22] J.E. Heebner, V. Wong, A. Schweinsberg, R.W. Boyd, D.J. Jackson, IEEE J. Quantum Electron. 40 (2004) 726–730.
[23] A.A. Savchenkov, A.B. Matsko, V.S. Ilchenko, L. Maleki, Opt. Express 15 (2007) 6768–6773.
[24] R. Loudon, M. Harris, T.J. Shepherd, Phys. Rev. A 48 (1993) 681–701.
[25] K. Totsuka, M. Tomita, Opt. Lett. 32 (2007) 3197–3199.
[26] J. Morville, D. Romanini, M. Chenevier, A. Kachanov, Appl. Opt. 41 (2002) 6980–6990.
[27] C. Dong, C. Zou, J. Cui, Y. Yang, Z. Han, G. Guo, Chin. Opt. Lett. 7 (2009) 299–301.
[28] S.T. Chu, B.E. Little, W. Pan, T. Kaneko, Y. Kokubun, IEEE Photon. Technol. Lett. 11 (1999) 1426–1428.
[29] T. Opatrný, D.G. Welsch, Phys. Rev. A 64 (2001) 023805.
[30] L. Maleki, A.B. Matsko, A.A. Savchenkov, V.S. Ilchenko, Opt. Lett. 29 (2004) 626–628.
[31] D.D. Smith, H. Chang, K.A. Fuller, A.T. Rosenberger, R.W. Boyd, Phys. Rev. A 69 (2004) 063804.
[32] A. Naweed, G. Farca, S.I. Shopova, A.T. Rosenberger, Phys. Rev. A 71 (2005) 043804.
[33] D.D. Smith, N.N. Lepeshkin, A. Schweinsberg, G. Gehring, R.W. Boyd, Q.-H. Park, H. Chang, D.J. Jackson, Opt. Commun. 264 (2006) 163–168.
[34] Q. Xu, S. Sandhu, M.L. Povinelli, J. Shakya, S. Fan, M. Lipson, Phys. Rev. Lett. 96 (2006) 123901.
[35] K. Totsuka, N. Kobayashi, M. Tomita, Phys. Rev. Lett. 98 (2007) 213904.
[36] Y. Dumeige, T.K.N. Nguyen, L. Ghisa, S. Trebaol, P. Féron, Phys. Rev. A 78 (2008) 013818.
[37] L.Y. Mario, M.K. Chin, Opt. Express 16 (2008) 1796–1807.
[38] M. Xiao, Y.-Q. Li, S.-Z. Jin, J. Gea-Banacloche, Phys. Rev. Lett. 74 (1995) 666–669.
[39] R. Tripathi, G.S. Pati, M. Messall, K. Salit, M.S. Shahriar, Opt. Commun. 266 (2006) 604–608.
[40] R.M. Camacho, M.V. Pack, J.C. Howell, Phys. Rev. A 73 (2006) 063812.
[41] D. Strekalov, D. Aveline, N. Yu, R. Thompson, A.B. Matsko, L. Maleki, J. Lightw. Technol. 21 (2003) 3052–3061.
[42] S. Poinsot, H. Porte, J.P. Goedgebuer, W.T. Rhodes, B. Boussert, Opt. Lett. 27 (2002) 1300–1302.
[43] V. Van, J. Lightw. Technol. 24 (2006) 2912–2919.
[44] Y. Dumeige, IEEE Photon. Technol. Lett. 21 (2009) 435–437.
[45] J.K.S. Poon, L. Zhu, J.M. Choi, G.A. DeRose, A. Scherer, A. Yariv, J. Opt. Soc. Am. B 24 (2007) 2389–2393.
[46] J. Scheuer, EPL 77 (2007) 44004.
[47] Y. Dumeige, EPL 86 (2009) 14003.
[48] Z. Shi, R.W. Boyd, R.M. Camacho, P.K. Vudyasetu, J.C. Howell, Phys. Rev. Lett. 99 (2007) 240801.
[49] Y. Dumeige, S. Trebaol, P. Féron, Phys. Rev. A 79 (2009) 013832.
[50] C. Peng, Z. Li, A. Xu, Appl. Opt. 46 (2007) 4125–4131.
[51] Y. Zhang, N. Wang, H. Tian, H. Wang, W. Qiu, J. Wang, P. Yuan, Phys. Lett. A 46 (2008) 5848–5852.